Available online at www.sciencedirect.com
ScienceDirect
International Journal of Heat and Fluid Flow 28 (2007) 2–14
International Journal of HEAT AND FLUID FLOW
www.elsevier.com/locate/ijhff

Single phase pressure drop in microchannels

Pega Hrnjak [a,*], Xiao Tu [b]

[a] Department of Mechanical Engineering, University of Illinois at Urbana Champaign, United States
[b] Microsoft Corporation, CA 98-1232, United States

Accepted 24 May 2006
Available online 27 October 2006

Abstract

This article focuses on investigating fully developed liquid and vapor flow through rectangular microchannels with hydraulic diameters varying from 69.5 to 304.7 μm and with aspect ratios changing from 0.09 to 0.24. R134a liquid and vapor were used as the testing fluids. During the experiments, the Reynolds numbers were varied between 112 and 9180. Pressure drop data are used to characterize the friction factor in the laminar region, the transition region and the turbulent region. When the channel surface roughness was low, both the laminar friction factor and the critical Reynolds number approached the conventional values, even for the smallest channel tested. Hence, there was no indication of deviation from the Navier–Stokes flow theory for rectangular microchannels. The friction factor data in the turbulent region were larger than the predictions from the [Churchill, S.W., 1977, Friction factor equations spans all fluid-flow regimes, Chemical Engineering 45, 91–92] equation for smooth tubes, even for the smoothest channel tested ($R_a/D_h = 0.14\%$). In addition, it was likely that surface roughness was responsible for higher laminar flow friction and earlier transition to turbulent flow in one of the channels tested.

1. Literature review

A summary of experimental studies of single-phase pressure drop in microchannels is listed in Table 1. Wu and Little (1983) measured the friction factor for the flow of gases in microchannels with hydraulic diameter ranging from 55.8 to 83.1 μm. They found that the friction factors for both the laminar and turbulent regimes were larger than predictions from the conventional equations. The transitional Reynolds numbers ranged from 350 to 900. The trend discovered was that rougher channels led to an earlier transition from laminar to turbulent flow. However, Wu and Little (1983) did not measure the surface roughness directly, instead, they estimated it using the Karman equation for the complete turbulent zone.

Peng et al. (1994) investigated experimentally the flow characteristics of water flowing through rectangular ducts having a hydraulic diameter of 133–367 μm and an aspect ratio of 0.333–1.0. Their experimental results indicated that the flow transition occurred between Reynolds numbers of 200–700. In addition, the flow friction behavior for both the laminar and turbulent flow dramatically deviated from the classical equations.

Choi et al. (1991) and Yu et al. (1995) measured friction factors for nitrogen and water flowing through micro tubes having inside diameters between 3 and 102 μm. The inner tube surfaces were described as ''molecularly smooth''. The measured friction factors in both laminar and turbulent region were found to be less than those predicted from the conventional correlations. The transitional Reynolds numbers were reported to be approximately 2000.

Flockhart and Dhariwal (1998) described the flow characteristics of distilled water flowing through trapezoidal channels with hydraulic diameters ranging from 50 to 120 μm. The Reynolds numbers were lower than 600 and the flow was kept well within the laminar flow regime. The experimental results were compared with numerical analysis results based on conventional fluid mechanics. The conventional theory was found to be able to predict

* Corresponding author. Tel.: +1 217 244 6377; fax: +1 217 333 1942.
E-mail address: pega@uiuc.edu (P. Hrnjak).

0142-727X/$ - see front matter © 2006 Published by Elsevier Inc.
doi:10.1016/j.ijheatfluidflow.2006.05.005

Nomenclature

Symbol	*description*	*units*
A	cross-section area	(m^2)
C_f	constant $= f \cdot Re$	(–)
D_h	hydraulic diameter	(m)
e	equivalent sand grain roughness	(m)
f	friction factor	(–)
G	mass flux	(kg/m^2 s)
g	gravitational constant	(m/s^2)
H	channel height	(μm, m)
h	heat transfer coefficient	(W/m^2 °C)
L_e	entrance length	(m)
L_i	exit length	(m)
L_t	total channel length	(m)
m	mass flow rate	(kg/s)
m	number of measurements	(–)
n	number of data points	(–)
p, P	pressure	(N/m^2)
R_a	arithmetic average surface roughness	(m)
Re	Reynolds number	(–)
R_p	maximum peak value of roughness	(m)
R_v	minimum valley value of roughness	(m)
T	temperature	(°C)
U, u	fluid velocity	(m/s)
W	channel width	(m)
x	vapor quality	(–)
z/D_h	hydraulic entrance length, dimensionless	(–)

Greek symbols

α	channel aspect ratio, H/W	(–)
α	void fraction	(–)
β	area ratio	(–)
ΔP, Δp	pressure drop	(N/m^2)
δ_{wall}	wall thickness	(m)
μ	viscosity	(kg/m s)
ρ	density	(kg/m^3)
ρ_{avg}	average density of homogeneous fluid	(kg/m^3)
σ	standard deviation	
σ	the area ratio	(–)
ψ_s	separated flow multiplier	(–)

the flow in microchannels; however, the authors did not report the surface roughness values.

Mala and Li (1999) studied flow characteristics of water flowing through stainless steel and fused silica microtubes with diameters ranging from 50 to 254 μm. The mean roughness height was ±1.75 μm, which was provided by the manufacturers. The authors did not provide the shape and the distribution of the roughness elements. For small Reynolds numbers, i.e., $Re < 500$, the experimental data were in rough agreement with the classical equation predictions. However, as the Reynolds number increased, the friction factor was significantly higher than the predictions by the conventional theory. The authors proposed two possible explanations. One is earlier transition from laminar to turbulent flow; and the other is the surface roughness effect.

Qu et al. (2000) conducted experiments to investigate frictional pressure drop of water flowing through trapezoidal microchannels with hydraulic diameters ranging from 51 to 169 μm. The channels were fabricated on silicon plates and covered with Pyrex glass covers. The cover was very smooth with an average surface roughness on the order of 10 nm, but the silicon channel had an averaged roughness ranging from 0.8 to 2.0 μm. The measured friction factors in the microchannels were higher (8–38%) than those given by the conventional flow theory. A roughness-viscosity model was proposed to interpret the experimental data.

Pfund et al. (2000) experimentally investigated the friction factors of water flowing through two parallel plates with a depth ranging from 128 to 521 μm and a fixed width

Table 1
Summary of single-phase studies in microchannels

Reference	Geometry	D_h (μm)	R_a/D_h (%)	Material	Re range	Re_c	Testing fluid
Wu and Little (1983)	Trapezoidal	55.8–83.1	0.5–30	Silicon, glass	100–15,000	350–900	N_2, H_2, Ar
Peng et al. (1994)	Rectangular (α: 0.333–1)	133–367	0.6–1	SS	50–4000	200–700	Water
Choi et al. (1991)	Circular	3.0–81.2	0.01–0.8	Silica	30–20,000	2300	N_2 gas
Yu et al. (1995)	Circular	19–102	0.03	Silica	250–20,000	2000	N_2 gas, water
Flockhart and Dhariwal (1998)	Trapezoidal	50–120	N/A	Silicon	⩽600	N/A	Water
Mala and Li (1999)	Circular	50–254	0.7–3.5	Fused silica, SS	80–2100	300–900	Water
Qu et al. (2000)	Trapezoidal	51–169	1.1–1.7	Silicon	0–1500	N/A	Water
Pfund et al. (2000)	Rectangular (α: 0.01–0.05)	252–973	0.02–0.4	Polycarbonate/ polyimide	40–4,000	1700–2200	Water
Judy et al. (2002)	Round, square	15–150	N/A	Fused silica, SS	8–2300	N/A	Water, methanol, isopropanol
Wu and Cheng (2003)	Trapezoidal	25.9–291.0	<0.12	Silicon	10–3000	1500–2000	Water

of 1-cm. Pressure drops were measured within the channel itself to exclude entrance and exit losses, and transitions to turbulence were observed with flow visualization. The experimental results suggest higher friction factors in laminar flow than the classical values. The transitions from laminar to turbulent flow occurred at Reynolds numbers that were lower than the critical Reynolds number for conventional ducts.

Judy et al. (2002) used the pressure drop data to characterize the friction factor for channel diameters in the range 15–150 μm and over a Reynolds number range 8–2300. The microchannels had round and square cross-section geometries. The authors found that error bounds are dominated by measurement of the diameter. The $f \cdot Re$ data revealed no distinguishable deviation from macroscale Stokes flow theory. However, no roughness information about the channel surfaces was reported.

Recently, Wu and Cheng (2003) conducted experiments to measure the friction factor of laminar flow of deionized water in silicon microchannels of trapezoidal cross-section with hydraulic diameters in the range of 25.9–291.0 μm. The relative roughness of all the channels was measured to be no more than 0.12%. The experimental data agreed within ±11% of the analytical solution based on the Stokes flow theory. The authors also reported that transition from laminar to turbulent flow occurred at $Re = 1500$–2000 in microchannels having triangular or trapezoidal cross-section with $D_h = 103.4$–291.0 μm.

The review of the literature exhibits large scatter and even contradictions in the experimental results for flow friction in microchannels. As has been pointed out by Pfund et al. (2000), the inconsistency in the reported results can be attributed to several factors such as channel size, geometry, and relative roughness, which were not measured or were possibly incorrectly determined. Since the bonding of silicon and glass is the principal method for microchannel fabrication (Wu and Little, 1983; Flockhart and Dhariwal, 1998; Qu et al., 2000), part of the discrepancy may be attributed to the lack of well-controlled surface structure during the bonding process. In addition, most of the studies did not measure pressures within the microchannel, but instead measured the pressure upstream and downstream of the channel, and applied conventional corrections for the inlet and exit losses. Unfortunately, it is still unknown whether these correlations can be used in microchannels. Furthermore, some investigators measured friction factors over a channel length of only about a hundred hydraulic diameters, which may not be sufficient length to allow for a fully developed flow.

Nevertheless, there is a general agreement in the literature that surface roughness is a very important factor for microchannel flow. When the channel was smooth, the flow transition from laminar to turbulent occurred at almost the same Reynolds number as the conventional results, according to Choi et al. (1991) and Yu et al. (1995). However, they reported friction factors in both the laminar and the turbulent region lower than the conventional results. The lower friction factor in the laminar and turbulent region may be due to the errors in tube diameter measurement, considering the smallest tube is only 3 μm in diameter and the measured friction factor is proportional to D^3. When the channel is rough enough, earlier transition and discrepancies from the conventional laminar friction factors were observed (Wu and Little, 1983; Mala and Li, 1999; Pfund et al., 2000).

Therefore, it is expected that the conventional correlations could be reproduced in microchannels providing the channel is smooth and the experiments are well controlled. Flockhart and Dhariwal (1998) reported such a result for channels as small as $D_h = 50$ μm and Reynolds number less than 600, however, they did not report the surface roughness. In order to better understand the flow behavior in microchannels, there is a need to perform extensive experiments with a larger range of Reynolds numbers, channel size and shape, and most importantly, with a wide range of surface roughness. The experimental results in the smoothest channels will provide a basis from which other work can be undertaken. The experimental data for rougher channels can be used to predict where the results move away from the basis.

Kandlikar et al. (2001) investigated the effect of channel roughness on flow friction in two tubes of 1.031 mm and 0.62 mm in diameter. The roughness of the inside tube surface was changed by etching it with an acid solution. They found that R_a/D of 0.3%, which may be considered smooth for tubes larger than 1 mm, increased the friction factor and heat transfer. The transition to turbulence also was affected by changing the roughness values above this limit.

The literature review also reveals that there is a lack of single-phase friction factor studies in microchannels for the following two topics: (1) Friction factors in rectangular microchannels. Peng et al. (1994) used rectangular microchannels but their results were dramatically different from other data as well as the conventional correlation predictions. It is not clear from the open literature whether the conventional correlations can be used in rectangular microchannels with hydraulic diameters close to or less than 100 μ. It also not clear what is the effect of aspect ratio, H/W, on the laminar flow friction factor and the critical Reynolds number. (2) Most of the studies, such as Flockhart and Dhariwal (1998), Mala and Li (1999), Qu et al. (2000), Judy et al. (2002) and Wu and Cheng (2003), focused most on the flow friction factor in the laminar region. There is a lack of study for flow friction in the turbulent region in microchannels.

In this work, attempts have been made to clarify the above two issues by measuring the frictional pressure drop of liquid and vapor R134a flowing through five rectangular channels with hydraulic diameters varying from 69.5 to 304.7 μm and aspect ratios changing from 0.09 to 0.24. The frictional pressure drops were measured within the channel, away from the entrance and the exit. The same test section was tested under both liquid and vapor state,

which provided a way to check the reliability of the experiment as well as to extend the experimental Reynolds number range to $Re = 112$–9180.

2. Test section

Five microchannel test sections with hydraulic diameters varying from 69.5 to 304.7 μm and with aspect ratios changing from 0.09 to 0.24 were designed and manufactured for single-phase investigation. These test sections were also used in the adiabatic two-phase pressure drop studies. In order to avoid the problem of maldistribution that is typically associated with a multiple-channel heat exchanger, single-channel test sections were designed and employed in the current study. The cross-section of such a channel is illustrated in Fig. 1. The test section consisted of two parts, a substrate on which a channel was machined and a cover plate. Both parts used a 6.4 mm thick clear PVC block. Using the transparent material enabled the same test section to be used for flow visualization in the future.

The surfaces of the cover plate and the substrate were very smooth ($R_a < 20$ nm) and flat. As a result, the test sections could be sealed easily by just bolting two surfaces together with balanced forces. As shown in Fig. 2, the spacing between the bolts was about 6 mm. This design is better than other methods of sealing such as O-ring or gasket, because it eliminated the possibilities of introducing an unknown gap between two surfaces. It also provided a well-controlled surface structure that is missed in other methods such as bonding. In addition, this design allowed easy disassembling and re-assembling of the test section; thus, the channel can be cleaned and the geometry can be measured anytime without damage.

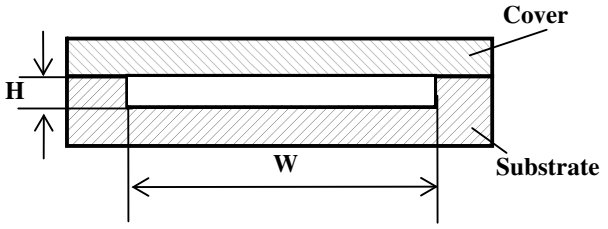

Fig. 1. Cross-section drawing of a microchannel test section used in pressure drop studies.

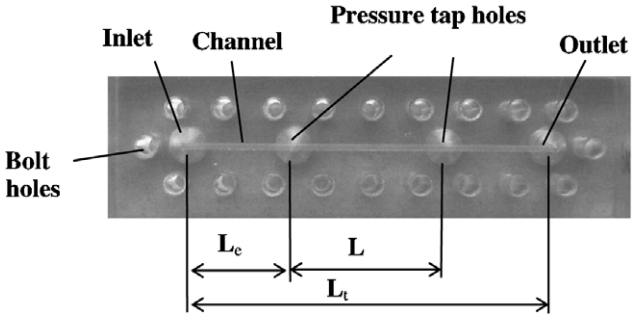

Fig. 2. Picture of a microchannel test section used in pressure drop studies.

As can be seen from Fig. 2, refrigerant flowed in and out of the channel through circular ducts with diameters equal to the channel width. These tubes were perpendicular to the channel and the entrance to the channel was abrupt. Two identical pressure tap holes, each with a diameter of less than 200 μm, were drilled in the center of the channel bottom, enabling direct measurement of the frictional pressure drops. The holes were checked under a microscope to make sure there were no burs around the edges.

Geometric parameters of the test sections are listed in Table 2. The length between the inlet and the first pressure tap hole, the entrance length (L_e/D_h), was selected such that the flow between the two pressure tap holes was fully developed. Since no guidance is available with regard to a proper entrance length for microchannels, the conventional results were used as a reference. For a fully developed turbulent flow, Obot (1988) suggests an entrance length, L_e/D_h, of 60. For laminar flow, the hydraulic entrance length (z/D_h) has been determined analytically and is found to be a linear function of the Reynolds number.

$$z/D_h = C_e Re \tag{1}$$

where C_e is a constant. For Reynolds numbers less than 2000, Hartnett et al. (1962) found that C_e to be 0.033 and 0.046, for rectangular channels of aspect ratio of 0.1 and 0.2, respectively. For Reynolds numbers larger than 2000, the flow is not completely laminar and the hydraulic entrance is less than the peak value at $Re = 2000$. Thus, for an aspect ratio of 0.2, the hydraulic entrance length over the entire Reynolds number is $z/D_h \leqslant 92$, which suggests that an entrance length (L_e/D_h) of about 92 would suffice for the current investigation. As seen from Table 2, this requirement was met for all the five test sections.

The channel lengths were measured with a Nikon MM-11 measurescope. The channel height and width were determined with a Sloan Dektak^3 ST stylus surface profilometer. Cross-section profile scans were performed across the microchannel at different locations along the length. Each scan generated 8000 data points at an interval of 0.25 μm, which created plots as shown in Fig. 3. The figure shows that the channel sidewalls are not perpendicular to

Table 2
Geometric parameters of the test sections

Test section	1	2	3	4	5
H (μm)	167.9	93.2	76.6	60.9	37.9
W (μm)	1646.7	383.5	889.2	359.2	416.5
H/W	0.10	0.24	0.09	0.17	0.09
D_h (μm)	304.7	150.0	141.1	104.1	69.5
L_t (mm)	96.0	48.0	48.0	48.0	48.0
L_e (mm)	28.0	14.0	14.0	14.0	14.0
L (mm)	40.0	20.0	20.0	20.0	20.0
L_e/D_h	92	93	99	135	203
L_t/D_h	315	320	340	460	691

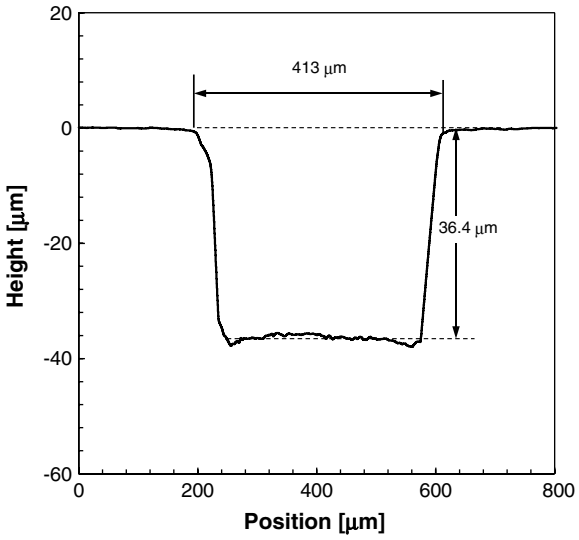

Fig. 3. Channel cross-section profile (test section #5).

the bottom surface. This is not the real shape of the channel; instead, the reason for the slant is that the stylus tip is installed on a triangular block. In reality, it is taken as a right angle according to the manufacturing technique used.

The surface profilometer has the capability of measuring step height down to a few nm. Hence, each scan could generate highly accurate data of the channel geometry at a specific location, and the channel height and width could be determined very accurately. However, the channel topography may not be the same at different locations, therefore, several measurements were taken and the averaged values were used. Such a result as well as the statistical data is listed in Tables 3 and 4. It shows that the microchannel cross-section geometry was quite consistent at different locations, and the channel could be considered as a straight duct. In order to check the repeatability of the average height (H) and average width (W), two separate groups of measurements were performed for test section #2 and #3 after the pressure drop experiment. The results were compared with the values in Tables 3 and 4, and the differences were within ±0.7%, for both H and W.

The Sloan Dektak[3] ST stylus surface profilometer was also used to characterize the channel surface roughness. As shown in Fig. 4, the channel cover plates were very smooth because it was not machined with a mean roughness of $R_a = 0.02$ μm, but the channel bottom surfaces were much rougher due to effect of machining, as shown in Fig. 5. Therefore, the microchannels had non-symmetric surface characteristics. The channel bottom roughness is reported as the arithmetic average surface roughness (R_a), the maximum peak value (R_p), as well as the minimum valley value (R_v) in Table 5.

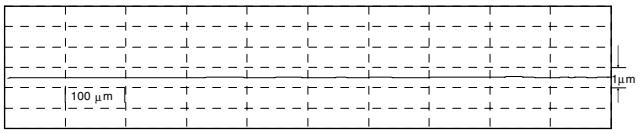

Fig. 4. Cover plate surface profile.

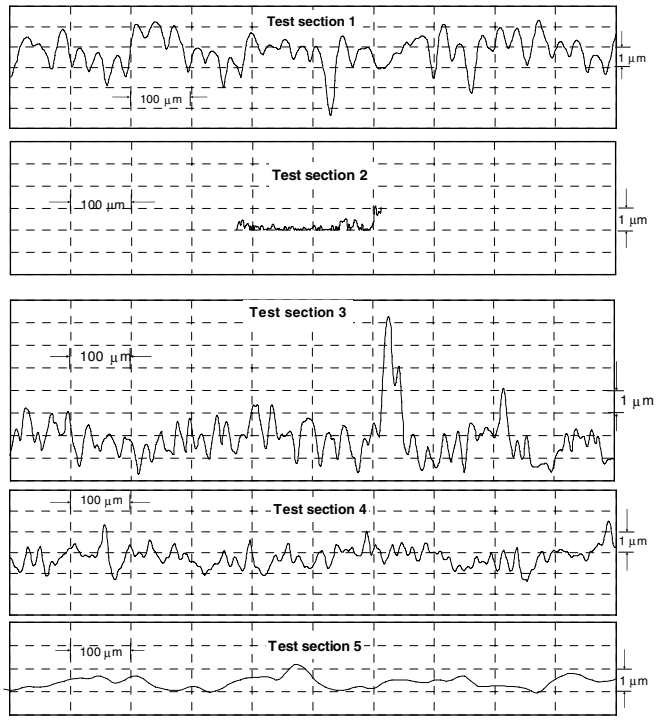

Fig. 5. Channel bottom surface profiles.

Table 3
Channel height measurement

Test section	1	2	3	4	5
Mean H (μm)	167.9	93.2	76.6	60.9	37.9
Standard deviation σ_H (μm)	1.1	1.3	0.4	0.4	1.0
Maximum H (μm)	169.8	95.7	77.4	61.4	39.4
Minimum H (μm)	166.2	91.4	76.1	60.4	36.4
Number of data	19	19	10	7	10

Table 4
Channel width measurement

Test section	1	2	3	4	5
Mean W (μm)	1646.7	383.5	889.2	359.2	416.5
Standard deviation σ_W (μm)	13.6	5.6	5.9	3.4	3.6
Maximum W (μm)	1676	392	898	364	420
Minimum W (μm)	1624	375	881	354	413
Number of data	19	11	21	7	10

Table 5
Channel bottom roughness measurement

Test section	1	2	3	4	5
R_a (μm)	0.48	0.21	0.48	0.30	0.21
R_p (μm)	2.3	0.8	2.4	1.5	0.77
R_v (μm)	2.4	0.7	2.0	1.1	1.10
R_a/D_h	0.16%	0.14%	0.35%	0.29%	0.30%
$2R_a/H$	0.57%	0.45%	1.25%	0.98%	1.11%

3. Experimental facility

The facility for the single-phase pressure drop study is shown in Fig. 6. Because the flow rate in microchannels is inherently small, the apparatus was designed as a once-through system for simplicity and flow stability. A tank containing refrigerant was heated with an electric resistance heater. A variable transformer was used to control the heating power, which in turn determined the saturation pressure of the refrigerant. The high-pressure refrigerant was driven from the bottom of the tank into the test loop as saturated liquid, which was cooled down to room temperature while flowing through the tubing to the test section.

Once leaving the refrigerant tank, the refrigerant flowed through two mass flow meters, one for larger flow rates (Micromotion model CMF010, m_2 in Fig. 6), and another for smaller flow rates (Rheotherm® model TU1/16, m_1 in Fig. 6). A filter with a mesh size of 0.5 μm was installed before the flow meters to protect them and the test section from dust particles. Because the Rheotherm® flow meter is based on liquid flow energy balance, a subcooler and a sight-glass was installed to make sure subcooled liquid entered the flow meter.

For the vapor tests, a receiver tank was placed into an ice-water bath, which provided a stable lower pressure. After the flow meters, the refrigerant flowed through a metering valve to control the flow rate. The refrigerant expanded in the metering valve, and turned into low pressure (or low temperature) two-phase flow. For most of the cases in the current study, the flow rate was so low that the refrigerant was brought to room-temperature vapor without the assistance of the heater. For some large flow rates, an electric heater was used to evaporate the refrigerant. After passing through the test section, the vapor was condensed in the receiver tank. The receiver ice-water bath was in a Dewar so that there was no condensation of water vapor outside of the bath that could decrease accuracy.

For liquid refrigerant tests, the receiver tank was exposed to room temperature. Metering valve #1 and heater #2 were by-passed and liquid R134a flowed directly to the test section. After passing through the test section, the refrigerant expanded to the pressure of receiver tank in metering valve #2.

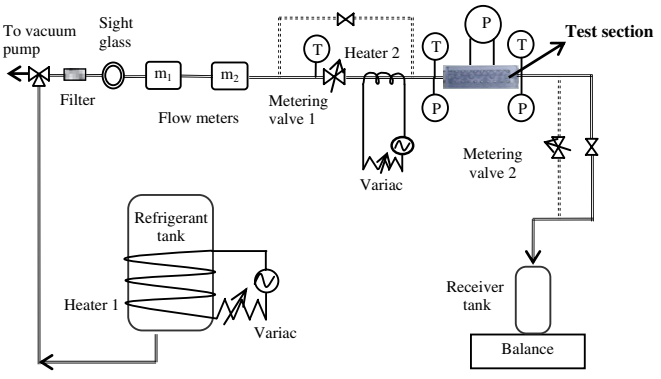

Fig. 6. Experimental facility for single-phase test.

3.1. Instrumentation

The receiver tank was placed above a digital balance (Sartorius model BP6100), which provides a third way to measure the mass flow rate in addition to the two flow meters mentioned above. The flow rate was measured by weighing the liquid accumulation during a period of stable state. The digital balance was connected to a computer with an RS-232 cable, which allowed the computer to retrieve the balance reading at intervals of three seconds. The slope function in Microsoft Excel, which returns the slope of the linear regression line through two groups of data points, was used to calculate the mass flow rate.

The mass flow rate in the current investigation spanned a range between 0.12–45.2 g/min. Mass flow rates larger than 8.5 g/min were measured using the Micromotion flow rate meter with an uncertainty of 0.7% according to the calibration curve supplied by the manufacture of the flow meter. The digital balance weighting method has been used to verify this uncertainty range, as shown in Fig. 6.

The flow rates below 8.5 g/min were measured with the digital balance. The uncertainties for flow rates below 8.5 g/min and above 0.36 g/min were within ±1.0%. For flow rate less than 0.36 g/min, at least 30 min of data were taken for a stable state, and the uncertainties were determined to be within ±2.0%.

The Rheotherm® flow meter operated in the range of 0.36 to 8.5 g/min. It was calibrated with the digital balance, as shown in Fig. 6, with an accuracy of ±3.0%. The experimental data within the operational region of Rheotherm were crosschecked with the flow rates determined from the balance reading, and the discrepancies were within ±3.0%. In addition, the continuous readings of this instrument provided an important means, in addition to the pressure and temperature versus time curves, to check whether a stable state had been reached.

The fluid temperatures at the inlet and outlet of the test section were measured with two type-T thermocouples. The test section inlet and outlet pressures were measured with two pressure transducers (Setra model 206, 0–1724 kPa). The pressure drop across the test section was measured with three differential pressure transducers (Setra model C230, 0–6.8 kPa, 0–68 kPa, and 0–172 kPa). All three transducers were used new and calibrated within an accuracy of 0.25% full scale by the manufacturer. Before the experiments, these three differential transducers were crosschecked in their overlapping region of operation. The crosschecking results confirmed the calibration results.

Measurements were recorded with a Hewlett–Packard (HP) data logger and a microcomputer. The sampling frequency was 20 times per minute, and the sampling time was no less than 5 min for each data point. All the data were recorded in Microsoft Excel for future processing.

4. Experimental procedure

The flow system was evacuated before it was charged with R134a. Prior to each experiment, air was bled from the test section, with particular attention being paid to remove air from the pressure tap ports since trapped air may induce noise in the measured pressure drop.

For liquid test, in order to make sure that the refrigerant was in a pure liquid state, most of the data points had inlet/outlet subcooling no less than 5 °C with the remaining no less than 0.5 °C. Similarly, most of the vapor data had inlet/outlet superheat larger than 5 °C with the remaining no less than 0.5 °C.

Each channel was tested with several runs of experiments. For a certain run, the Reynolds number changed either from smaller flow rates to larger ones or vice versa. Since the Reynolds number is a similarity parameter, it is expected that the f versus Re relationship should not be a function of experimental conditions such as absolute pressure of fluids, fluid state (liquid or vapor), flow direction (since the channel was symmetric), as well as whether the experiment is running from larger Reynolds numbers to smaller ones or vice versa. In addition, it should not matter if the channel is taken apart and put together again. These experimental conditions were kept unchanged in a certain experimental run, but varied extensively between different runs. No systematic differences observed between different groups of data suggest proper design of the test section, the experimental methods, as well as correct data reduction techniques.

The microchannel surface may have been deflected during the experiments because of high test-section pressure. Since the height of the microchannel was as small as 37.9 μm, even a deflection of 1 μm in height may introduce noticeable differences (about 10%) in measured friction factors. The deflection is a strong functions of the fluid pressure, i.e., the higher the pressure the larger the deflection. The current test section was designed such that the deflection was expected to be negligible. During the current experiment, the averaged test section pressure for liquid data varied between 655 kPa and 1065 kPa for different runs. No indications of friction factor dependence on the test section pressure were observed.

For $m < 0.36$ g/min, the digital balance is used to measure the mass flow rate. The accuracy of this approach depends greatly on the stability of the flow. When the experiments were performed with increasing Re or decreasing Re (closing or opening valve), the flow rates would have a tendency of increasing or decreasing before a stable state has been established. If the data were taken at this stage, systematic errors could be observed. Different runs of data were compared for the current investigation and no systematic errors were observed.

If the fine channel was contaminated with particles, unexpected experimental results may have appeared. Test section #3 and #4 were uncovered and cleaned between different runs, and no systematic errors were observed.

All these efforts verified our design of experiments and greatly improved the quality of the experimental data.

4.1. Experimental results

The experimental facility, instrumentation, experimental procedure, data reduction and uncertainties, as well as the characterization of the microchannel test sections are described in Tu and Hrnjak (2004).

Hartnett and Kostic (1989) give the following simple equation, which is within 0.05% of the analytical solution of a Newtonian fluid in fully developed laminar flow through rectangular ducts.

$$\begin{aligned} C_f &= f \cdot Re \\ &= 96(1 - 1.3553\alpha + 1.9467\alpha^2 - 1.7012\alpha^3 \\ &\quad + 0.9546\alpha^4 - 0.2537\alpha^5) \end{aligned} \tag{2}$$

The experimental results for all the test sections are shown in Figs. 7–11. In each figure, part (a) represents the friction factor, f, for the entire Reynolds number range in the form of f versus Re log–log plot; and part (b) presents the product $f \cdot Re$ as a function of the Reynolds number for data with $Re < 3000$. The circles and the crosses represent the experimental data for the liquid and vapor state, respectively. The dashed lines in part (a) show the theoretical results for fully developed laminar flow in

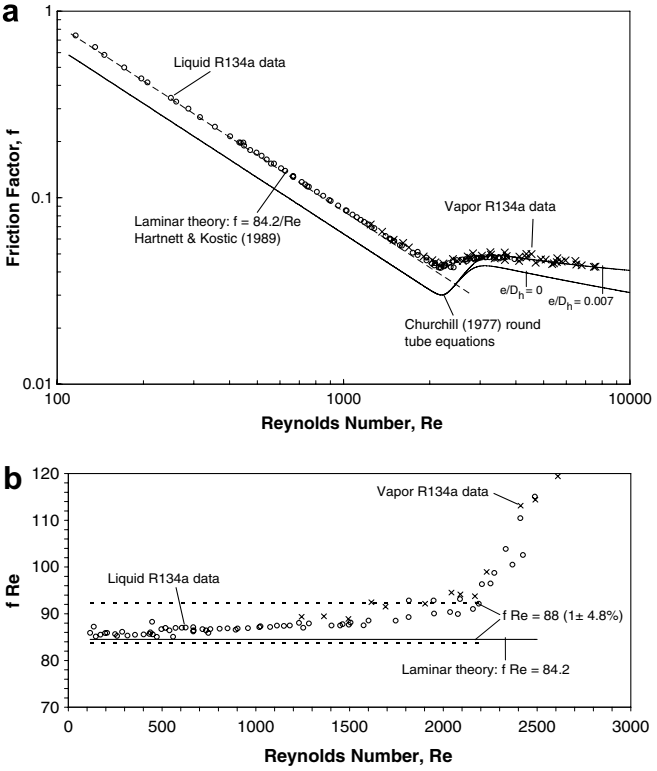

Fig. 7. Friction factor for test section #1 ($D_h = 305$ μm, $H/W = 0.1$).

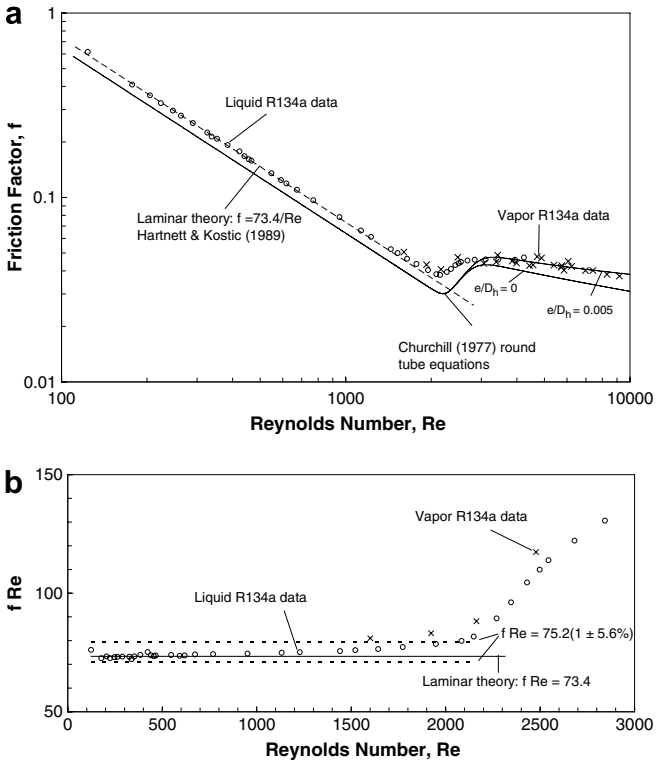

Fig. 8. Friction factor for test section #2 ($D_h = 150$ μm, $H/W = 0.24$).

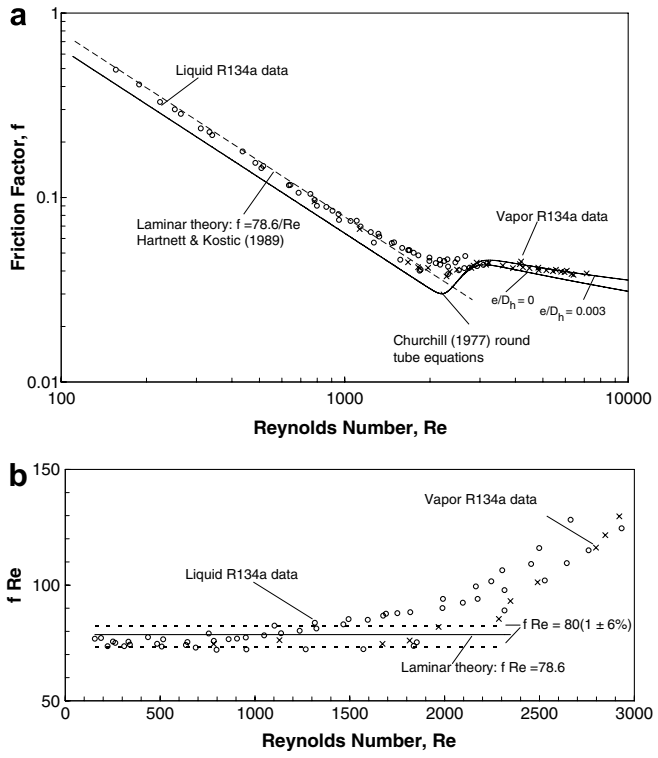

Fig. 10. Friction factor for test section #4 ($D_h = 104$ μm, $H/W = 0.17$).

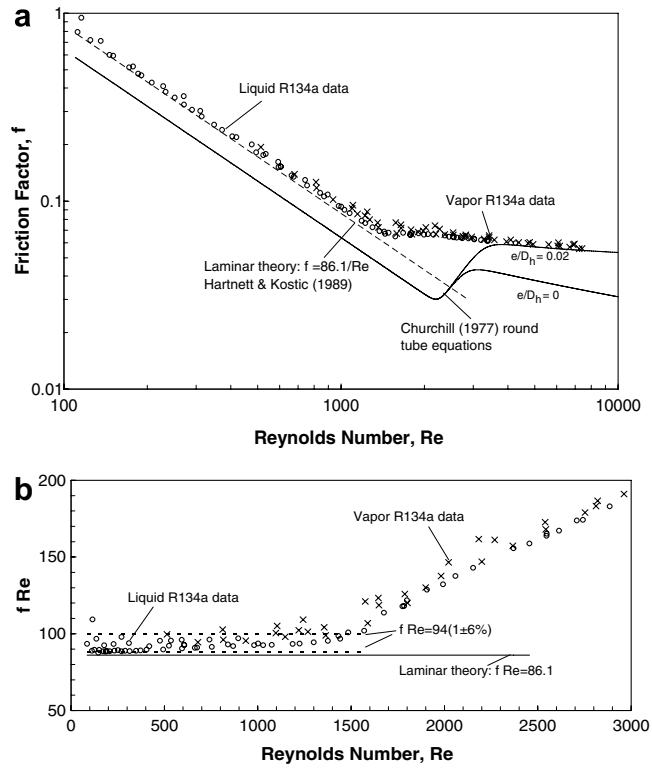

Fig. 9. Friction factor for test section #3 ($D_h = 141$ μm, $H/W = 0.09$).

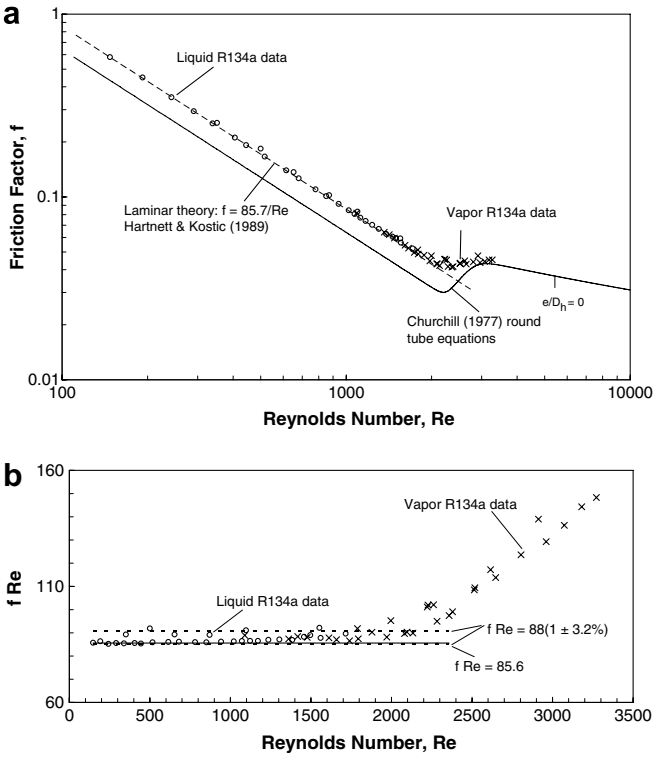

Fig. 11. Friction factor for test section #5 ($D_h = 69$ μm, $H/W = 0.09$).

rectangular channels, Eq. (2). The solid lines are the Churchill (1977) equations for round tubes with different relative roughness (e/D).

As seen from Figs. 7–11, the liquid data and the vapor data collapse on the same curve. Considering two data points with the same Reynolds number, one in the liquid

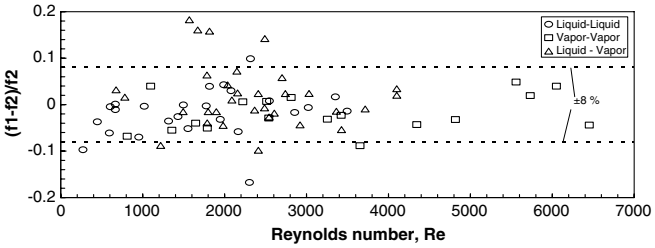

Fig. 12. Repeatability of f vs. Re relationship.

state and the other in the vapor state, the mass flow rate for the liquid state is typically 20 times that of the vapor one. Additionally, the measured frictional pressure drop for the liquid state is normally about three times larger than that of the vapor data. In addition, the test section pressure for the liquid state is much higher than that of the vapor state. Thus, the consistency of the data for liquid and vapor state verified the soundness of the experimental methods.

Among the 468 data points shown in Figs. 7–11, seventy-five pairs have the same Reynolds number. It should be noted that two Reynolds numbers with differences within ±1% were considered equal. The difference of the measured friction factors was calculated for each pair, and shown as a function of Reynolds number in Fig. 12. The data label liquid–liquid and vapor–vapor represent both data points in liquid state or vapor state, respectively. Liquid–vapor means two data points, one in liquid and another in vapor state, have the same Reynolds number. Note that the pairs of data are from different runs, as addressed in the experimental procedure section.

For data pairs with the same state (liquid–liquid or vapor–vapor) in Fig. 12, 91.0% of the points are within ±8%. For liquid–vapor pairs, 88% of the points lay within ±10%. Considering the maximum uncertainty of measured friction factor (±6.2%) and the variety of experimental conditions that has been changed for different runs, as well as the ±1.0% error for the Reynolds number, this is in very good agreement. In addition, most of the large errors reside in the region of $1500 < Re < 2500$ Fig. 12. This is the region where the flow transition from laminar to turbulent occurs, which may be the reason for the scatter of the data points.

5. Analysis and discussions

5.1. Flow regions

Test section #1 has the largest hydraulic diameter among all the channels. As seen in Fig. 7(a), at low Reynolds number range ($Re < 2190$), the measured friction factors decrease linearly with Reynolds number on a log–log plot. This is the laminar flow region. At $Re = 2190$, the measured friction factors reach the local minimum value ($f \approx 0.04$) and start to deviate from the laminar data. After that, the friction factor rises with increasing Reynolds number in the intermediate Reynolds number range ($2190 < Re < 3000$), following a trend that has been reported for large pipes and channels. This is the critical region. The Reynolds number (2190) at which the friction factor starts to break from the laminar flow line, is called the critical Reynolds number. When the Reynolds number is larger than 3000, the friction factors decrease slowly with Reynolds number. This is the turbulent flow region.

Similarly, the f versus Re results for test section #2 and #4 can be divided into the three regions, the laminar region, the critical region and the turbulent region (see Figs. 8 and 9). For test section #5, the current experimental facility and methods limit the experimental Re to less than 3272, and only the laminar region and the critical region can be seen from Fig. 11(a). There is no clear indication of the critical region for test section #3, as seen in Fig. 9, which suggests a sudden transition from laminar to turbulent flow.

5.2. Laminar flow friction factor

Figures 7(b)–11(b) show the product $f \cdot Re$ versus Re for data with Reynolds number less than 3500 in linear coordinates. In these figures, the solid lines mark the theoretical predictions based on Eq. (2). For each test section, the average of all the laminar data was calculated, and multiplied by one plus the uncertainty of $f \cdot Re$ (see Table 6). The results are represented in Figure 7(b) to 11(b) as two dashed lines. Most of the laminar flow data nicely lay between the two dashed lines, with a few data points close to the critical point as exceptions. Therefore, to the degree of the current experimental uncertainties, the product $f \cdot Re$ is a constant value in the laminar flow region, which is consistent with the conventional results.

The mean values of $f \cdot Re$ in the laminar region were taken as the experimental friction factor constant and compared with the theoretical predictions based on Eq. (2), as shown in Fig. 13 and Table 6. In section 2.2.5 of Tu and Hrnjak (2004); the error of $f \cdot Re$ associated with the channel geometry measurements were determined to be within ±2.8% for all the five test sections. This is shown in Fig. 13 as error bars.

The measured values of the friction constants were higher than the classical results for all the five channels. However, the differences for the four test sections other than #3 were small (less than 4%) and were attributed to the uncertainties associated with height and width measurement. Fig. 13 indicates that the effect of aspect ratio, H/W, on the laminar flow friction constant, $f \cdot Re$, in rect-

Table 6
Single-phase friction factor experimental results vs. conventional values

Test	D_h	H/W	$(f \cdot Re)/(f \cdot Re)_{conv}$	$Re_c/Re_{c,conv}$
1	304.7	0.10	88.0/84.5	2190/2,470
2	150.0	0.24	75.2/73.4	2150/2315
3	141.1	0.09	94.0/86.1	1570/2470
4	104.1	0.17	80.0/78.6	2290/2315–2470
5	69.5	0.09	88.0/85.6	2200/2470

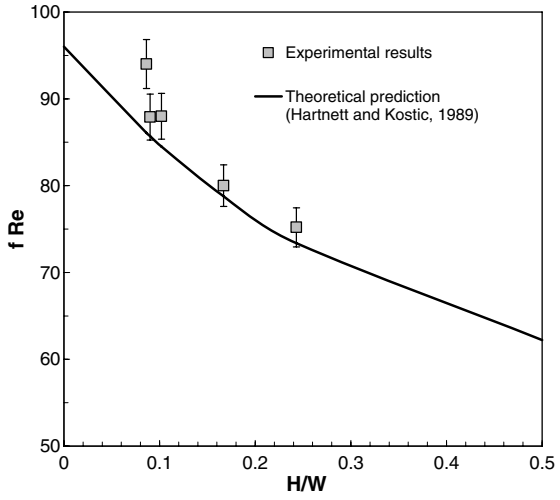

Fig. 13. Measured friction factor constants vs. theoretical predictions.

angular microchannels follows that of the conventional results, Eq. (2). The only exception is for test section #3 that has an $f \cdot Re$ value about 9% higher than the prediction of Eq. (2).

5.3. Critical reynolds number

The experimental critical Reynolds numbers are compared with those in conventional channels having abrupt entrances (Obot, 1988), as shown in Table 6. It should be noted here that a matching conventional result is not available for an aspect ratio of 0.17. However, according to Obot (1988), the tendency is that the smaller the aspect ratio, the larger the critical Reynolds number. Therefore, a first estimate of the conventional value for aspect ratio of 0.17 would be within the range of $2315 < Re_c < 2470$.

The current experiments suggest slightly earlier transition from laminar to turbulent for all the test sections. Although this tendency is consistent with the majority of the previous research results in microchannels (Wu and Little, 1983; Peng et al., 1994; Mala and Li, 1999; Pfund et al., 2000), the present critical Reynolds numbers approach the macroscale results. This is true especially for test section #1, #2, #4, and #5. Critical Reynolds numbers in the range of $200 < Re_c < 900$ for microchannels, as has been reported in Wu and Little (1983), Peng et al. (1994) and Mala and Li (1999), were not observed in the current study.

5.4. Turbulent flow friction factor

Hartnett et al. (1962) found that the circular-tube correlation accurately predicts the friction coefficient for flow through smooth rectangular ducts of any aspect ratio for $Re = 6 \times 10^3$–5×10^5. For rough tubes, it is well known that the relative roughness e/D, where e is the sand grain size, is a major parameter on the flow characteristics. The relative roughness, e/D, for a specific channel can be determined indirectly from the value of the friction factor in the completely turbulent zone. In this zone, the curve of f appears as a set of horizontal lines. The values of f depend only on the relative roughness, and the Karman equation can be used to estimate the e/D, as has been done by Wu and Little (1983). Obviously, such a region has not been reached in the current experiment, since the friction factor decreases with Reynolds number even for the largest Reynolds number tested ($Re = 9180$).

As shown in Figs. 7–11, the friction factors in the turbulent region do not follow the smooth tube correlation (Churchill, 1977). Instead, in the regions of $Re > 3000$, they follow the Churchill's equation with relative roughness e/D of about 0.7%, 0.5%, 2.0% and 0.3% for test section #1, #2, #3 and #4, respectively.

Even for the smoothest channel, test section #2 ($R_a/D_h = 0.14\%$), the turbulent friction factors are up to 30% larger than the Churchill's equation with $e/D = 0$. In conventional channels, however, a roughness of $R_a/D_h = 0.14\%$ can be considered as smooth. The results show that the condition of hydraulic smoothness is more difficult to satisfy in microchannels. A similar trend has been described in Acosta et al. (1985) for microchannels with a hydraulic diameter of 368.9 μm. They reported that the condition of hydraulic smoothness in the turbulent regime could be satisfied only when the walls were "optically smooth". Thus, the present result suggests that it may not be proper to call a microchannel with relative roughness of 0.12% as "smooth" channel, as has been done by Wu and Cheng (2003).

5.5. Discussions on the effect of roughness

As seen in Table 5 the R_a/D_h value for test section #3 (0.35%) is larger than that of test section #2 (0.14%) and #1 (0.16%). This difference may not be significant in conventional channels, but it can have a dramatic effect on the turbulent flow friction factor in microchannels. As it can be seen from Figs. 7–9, in the regime of $Re > 3000$, the friction factor of channel #3 is about 20–30% larger than that of channel #1 and #2.

In addition to this, channel #3 demonstrates unusual behavior in the laminar regime and the transition region when compared with other channels and the conventional results; i.e., the laminar friction factor is larger than theoretical predictions and the transition to turbulent is much earlier than other channels. Extensive efforts have been made to eliminate the possibilities that this is due to some unconsidered experimental errors. For example, the channel has been opened and cleaned three times between different runs of experiments. The flow direction has been reversed for one group of data. The 125 experimental data shown in Fig. 9 contain six different runs with two runs conducted four months after the first run. As has been analyzed previously, these experimental runs report repeatable f versus Re relationship. In addition, as shown in Tables 3 and 4, this channel has well-controlled and consistent

topographies at different locations. The channel entrance and the pressure tap holes were observed carefully under a microscope, and no burs were observed. Therefore, we have confidence in the experimental results for channel #3.

Channels #3 and #1 can be considered geometrically similar; that is to say, they have almost the same value of L_e/D_h, L_t/D_h, H/W and even contraction ratio (supplying pipe area divided by the channel cross-section area). The only differences are the channel sizes and the surface roughness. In large channels, the critical Reynolds number depends on many factors including the channel shape (round or rectangular, aspect ratio), the entrance condition (smooth or abrupt), initial flow condition, surface roughness, as well as the entrance length, L_e/D_h (Obot, 1988). The fact that these two channels are geometrically similar indicates that the difference in surface roughness may be the reason for the disagreement between the two critical Reynolds numbers. It is well known that transition can be delayed to larger Re if the necessary precautions (no disturbance at inlet, no pipe vibration, etc.) are taken. During the current experiment, no special precautions were taken to delay the transition. Therefore, the earlier transition from laminar to turbulent flow in channel #3 than in channel #1 could be attributed to a larger relative roughness, R_a/D_h, in channel #3. Wu and Little (1983) and Mala and Li (1999) reported earlier transition to turbulent flow in rough microchannels. However, as show in Table 1, their observation was based on larger values of R_a/D_h (>0.5%). The current results indicate that the transition behavior in microchannels could be different when the value of R_a/D_h is equal to or larger than 0.35%.

Channel #6 has nearly the same aspect ratio as channels #1 and #3. The critical Reynolds numbers of channels #1 and #6 are almost the same, but are larger than channel #3. The difference (or similarity) in flow transition among these three channels could be attributed to the combined effect of surface roughness and entrance length. The R_a/D_h value of channel #6 (0.3%) is larger than that of channel #1 (0.16%) but less than that of channel #3 (0.35%). Channel #6 is not geometrically similar to channel #1 and #3. As seen in Table 2, the entrance length (L_e/D_h) of channel #6 is more than twice the values of channel #1 and #3. In conventional channels, Obot (1988) summarized many examples of entrance length on critical Reynolds number. Therefore, even though the R_a/D_h value of channel #6 is only slightly less than channel #3, the critical Reynolds number is very different.

The parameter R_a/D_h may not be the best measure of surface roughness in microchannels. As seen in Fig. 5, although channels #3 and #5 have very close values of R_a/D_h, the distribution and shape of the roughness elements are very different. For example, in the same 100 μm distance, the surface of channel #3 has more occurrences of peaks and valleys. Channel #3 has one peak value of about 5 μm height, which is about ten times the value of R_a for this channel. Considering the channel height of 77 μm, this roughness element is about 6.5% of the channel height. At several other locations, roughness elements with close to ten times R_a were evident in the profilometry results of channel #3, but not observed in other channels. For this reason, channel #3 is "rougher" than the R_a/D_h value indicates when comparing with other channels. Another example is that channels #2 and #5 have the same value of R_a (0.21). However, they look different in the distribution and shape of their roughness elements.

The effect of roughness in microchannels is not only limited to the flow transition and turbulent flow region. As has been reported by Wu and Little (1983), Pfund et al. (2000), and Qu et al. (2000), the laminar friction factors may be larger than the theoretical predictions in rough microchannels. For channel #3, the mean value of the friction factor in the laminar region is about 9% higher than the classical predictions, which is greater than the possible experimental uncertainties. The higher friction factor may be attributed to a large roughness in this channel. Guo and Li (2003) also pointed out that due to the fact that the microchannels have a large surface to volume ratio, factors related to surface effects have more impact to the flow at small scales and surface roughness is likely responsible for the early transition from laminar to turbulent flow and the increased friction factor in microchannels.

5.6. Data reduction and uncertainties

The friction factor (f), Reynolds number (Re), and friction factor constant ($f \times Re$) were determined for each data point. The Reynolds numbers were calculated based on the hydraulic diameter of the channel:

$$Re = \frac{GD_h}{\mu}$$

The mass flux (G) and the hydraulic diameter (D_h) were calculated with the following equations:

$$G = \frac{m}{H \times W}, \quad D_h = \frac{2HW}{H + W}$$

Liquid flow was assumed incompressible, and the friction factor was calculated as,

$$f = \Delta P \frac{D_h}{L} \frac{2\rho}{G^2}$$

Substituting earlier equations we get

$$f = \frac{4\rho \times \Delta P \times H^3 W^3}{L(H + W)m^2}$$

$$C_f \equiv f \times Re = \frac{8\rho \Delta P H^3 W^3}{L\mu(H + W)^2 m}$$

The vapor flow in so small a channel cannot be taken as incompressible. Based on the momentum theorem, the pressure drop while gas flows in a straight constant area channel is

$$\frac{dp}{dx} = -\frac{f}{D_h}\frac{\rho u^2}{2} - \rho u \frac{du}{dx}$$

Table 7
Experimental uncertainties of single-phase pressure drop test

Parameters	Uncertainty
m (0.2–0.36 g/min)	±2.0%
m (0.36–8.5 g/min)	±1.0%
m (>8.5 g/min)	±0.7%
Absolute pressure	±3.5 kPa
Temperature	±0.2 °C
Differential pressure (0–6.8 kPa)	±0.017 kPa
Differential pressure (6.8–172 kPa)	±0.43 kPa

Table 8
Error propagation of single-phase pressure drop test

Test section	Re (%)	f (%)	C_f (%)
1	±1.0	±5.1	±4.8
2	±2.0	±5.9	±5.6
3	±2.0	±6.3	±6.0
4	±2.0	±6.0	±5.8
5	±2.0	±4.5	±3.2

The above equation can be integrated assuming isothermal, ideal gas flow, that is,

$$p_1 - p_2 = \frac{G^2}{2\rho_m}\left(f\frac{L}{D_h} + 2\ln\frac{p_1}{p_2}\right)$$

where ρ_m is the density based on the average pressure $(p_1 + p_2)/2$.

The uncertainties for the measured parameters and the calculated results are listed in Tables 6 and 7, respectively. The uncertainty propagation functions were used to estimate uncertainties for calculated results. Although each data point has an associated uncertainty, only the maximum values of the uncertainties are presented for each test section.

The above uncertainty analysis did not consider the errors introduced from the channel geometry (length, height, and width) measurements. The geometric parameter errors, when propagated into calculated results, are systematic. For example, a positive error in channel height would increase the entire calculated friction factors, f, of that channel for the same percentage. In the f versus Re curves discussed below, it will shift the entire data up/down and left/right, without changing the shape of the curve. As a result, the uncertainty propagations of these parameters are analyzed separately Table 8.

The error associated with the channel length was neglected since it could be measured very accurately (within ±0.1% error). The repeatability of H and W were within ±0.7% and the maximum errors for Re, f and $f \cdot Re$ associated with these two parameters were ±0.7%, ±3.5%, and ±2.8%, respectively.

6. Summary and conclusions

Fully developed flow frictional pressure drops have been measured over a Reynolds number range of $112 \leqslant Re \leqslant 9180$ for rectangular microchannels in the hydraulic diameter range of $69.5\ \mu m \leqslant D_h \leqslant 304.7\ \mu m$, in the height-to-width ratio range of $0.09 \leqslant \alpha \leqslant 0.24$, and in the relative roughness range of 0.14–0.35%.

The experimental methods are summarized as follows: (1) The test sections were sealed by pressing two smooth surfaces gently with bolts; thereby the channel geometry being tested could be considered the same as when it is open for measurements. (2) The frictional pressure drop was measured directly with pressure ports inside the channel. (3) The fully developed flow was established for the entire Reynolds number range with an adequate entrance length. (4) In order to check the repeatability of the measured friction factor versus Reynolds number relationship, the experimental conditions (test section pressure, fluid state, approaches to the desired flow rate, uncovering channel, etc.) that are believed to be unrelated to the f versus Re curve were varied extensively in different runs.

The following conclusions are obtained from this experimental investigation. (1) In the laminar region, the experimental data for frictional constants, $f \cdot Re$, of both liquid and vapor R134a flow in four microchannels with smoother surfaces ($R_a/D_h < 0.3\%$) agree with the analytical solution based on the Navier–Stokes equation, and the effect of aspect ratio presented in the correlation by Hartnet and Kostic, (1989) works for small channels (Fig. 13). (2) The critical Reynolds numbers of the above four smoother microchannels were in the range of $2150 \leqslant Re_c \leqslant 2290$, which are only marginally earlier than the conventional results for rectangular channels with the same aspect ratios. (3) In the turbulent region, the friction factors in all the microchannels tested are considerably larger than that predicted by the Churchill's (1977) equations for smooth tubes. Even for the smoothest channel with relative roughness of 0.14% the turbulent friction factors are up to 30% larger than the Churchill's equation with $e/D = 0$. (4) For one channel with the greatest surface roughness, $R_a/D_h = 0.35\%$, but intermediate hydraulic diameter, $D_h = 141.1\ \mu m$, the friction factor data showed different behaviors in the entire range of experiments. The laminar friction was about 9% higher than the theoretical predictions; the critical Reynolds number, $Re_c = 1570$, was earlier than the conventional results; and the turbulent friction was higher than other channels. The unusual behavior was an indication of the effect of surface roughness in microchannels.

References

Acosta, R.E., Muller, R.H., Tobias, C.W., 1985. Transport processes in narrow (capillary) channels. AICHE Journal 31 (3).

Choi, S.B., Barron, R.F., Warrington, R.O., 1991. Fluid flow and heat transfer in microtubesMicromechanical Sensors, Actuators, and Systems, DSC-vol. 32. ASME, pp. 123–134.

Churchill, S.W., 1977. Friction factor equations spans all fluid-flow regimes. Chemical Engineering 45, 91–92.

Flockhart, S.M., Dhariwal, R.S., 1998. Experimental and numerical investigation into the flow characteristics of channels etched in ⟨100⟩ silicon. Journal of Fluids Engineering 120, 291–295.

Guo, Z.Y., Li, Z.X., 2003. Size effect on microscale single-phase flow and heat transfer. International Journal of Heat and Mass Transfer 46 (1), 149–159.

Hartnett, J.P., Kostic, M., 1989. Heat transfer to Newtonian and non-Newtonian fluids in rectangular ducts. Advances in Heat Transfer 19, 247–356.

Hartnett, J.P., Koh, J.C.Y., McComas, S.T., 1962. A Comparison of predicted and measured friction factors for turbulent flow through rectangular ducts. Transactions of the ASME (February), 82–88.

Judy, J., Maynes, D., Webb, B.W., 2002. Characterization of frictional pressure drop for liquid flows through microchannels. International Journal of Heat and Mass Transfer 45, 3477–3489.

Kandlikar, S.G., Joshi, S., Tian, S., 2001. Effect of channel roughness on heat transfer and fluid flow characteristics in narrow channels, ASME National Heat Transfer Conference, Los Angeles, CA.

Mala, G.M., Li, D., 1999. Flow characteristics of water in microtubes. International Journal of Heat and Fluid Flow 20, 142–148.

Obot, N.T., 1988. Determination of incompressible flow friction in smooth circular and noncircular passages: a generalized approach including validation of the nearly century old hydraulic diameter concept. Journal of Fluids Engineering 110, 431–440.

Peng, X.F., Peterson, G.P., Wang, B.X., 1994. Frictional flow characteristics of water flowing through microchannels. Experimental Heat Transfer 7, 249–264.

Pfund, D., Rector, D., Shekarriz, A., Popescu, A., Welty, J., 2000. Pressure drop measurements in a microchannel. AICHE Journal 46 (8), 1496–1507.

Qu, W.L., Mala, G.M., Li, D.Q., 2000. Pressure-driven water flows in trapezoidal silicon microchannels. International Journal of Heat and Mass Transfer 43, 353–364.

Tu, X., Hrnjak, P., 2004. Flow and heat transfer in microchannels 30 to 300 microns in hydraulic diameter. ACRC report CR5X.

Wu, H.Y., Cheng, P., 2003. Friction factors in smooth trapezoidal silicon microchannels with different aspect ratios. International Journal of Heat and Mass Transfer 46, 2519–2525.

Wu, P.Y., Little, W.A., 1983. Measurement of friction factors for the flow of gases in very fine channels used for microminiaturize Joule–Thomson refrigerators. Cryogenics 24 (8), 273–277.

Yu, D., Warrington, R., Barron, R., Ameel, T., 1995. An experimental and theoretical investigation of fluid flow and heat transfer in microtubes. In: ASME/JSME Thermal Engineering Conference, vol. 1, pp. 523–530.